Supplemental Figures

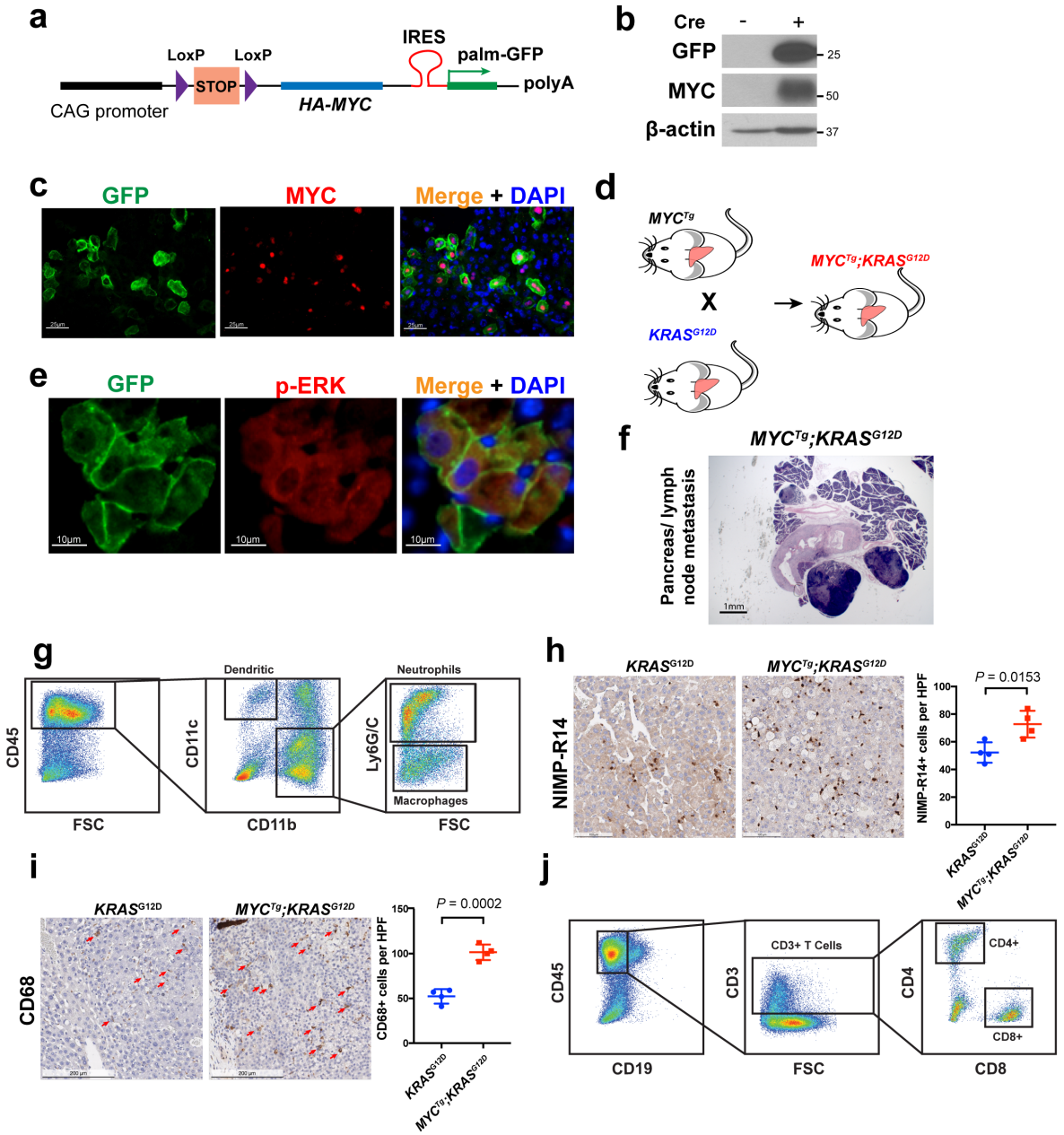

Supplementary Figure 1 Generation and characterization of *Alb Cre; KRAS^{G12D}* and *MYC^{Tg};KRAS^{G12D}* mice.

(a) Construct for inducible expression of *MYC* transgene.

(b) GFP and MYC protein expression in the liver of Adenoviral-Cre infected *MYC^{Tg}* mice (via tail vein) were assessed by western blot.

(c) GFP and MYC protein expression in the liver of Adenoviral-Cre infected *MYC^{Tg}* mice were assessed by immunofluorescence.

(d) *Alb Cre; MYC^{Tg};KRAS^{G12D}* mice were generated by intercrossing *MYC^{Tg}* mice with *KRAS^{G12D}* mice, followed by crossing with *Alb Cre* mice.

(e) Co-expression of GFP (indication of MYC expression) and p-ERK (indication of the activation of RTK/RAS signaling) were detected by immunofluorescence in *Alb Cre; MYC^{Tg};$KRAS^{G12D}$* mice liver tissue. Representative figure from n=3 independent experiments is shown.
(f) Representative *MYC^{Tg};$KRAS^{G12D}$* mice histology (n=4) of lymph node metastasis.
(g) Flow cytometry graph showing the strategy for distinguishing dendritic cells, neutrophils and macrophages.
(h) Representative and quantitative immunohistochemical analysis of NIMP-R14 (neutrophil marker) in *$KRAS^{G12D}$* (n=4 animals) and *MYC^{Tg};$KRAS^{G12D}$* (n=4 animals) mice liver tumors. Two-sided *t*-test.
(i) Representative and quantitative immunohistochemical analysis of CD68 (macrophage marker) in *$KRAS^{G12D}$* (n=4 animals) and *MYC^{Tg};$KRAS^{G12D}$* (n=4 animals) mice liver tumors. Red arrows represent CD68+ cells. Two-sided *t*-test.
(j) Flow cytometry graph showing the strategy for distinguishing CD4+ and CD8+ T lymphocytes.
All values represent the mean ± SD. Uncropped blots are provided in Supplementary Figure 15.

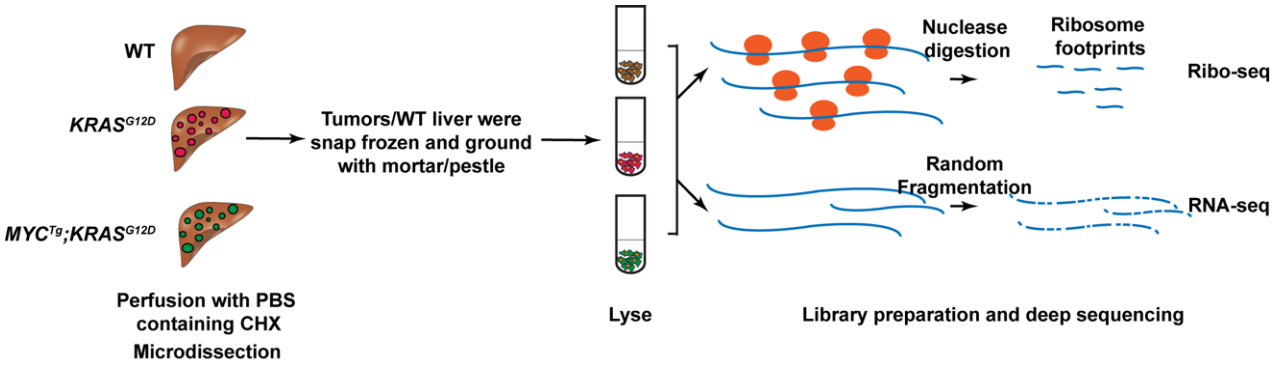

Supplementary Figure 2 Identifying the gene expression landscapes in WT liver, *KRAS*^{G12D} and *MYC*^{Tg}*;KRAS*^{G12D} mice liver tumors using ribosome profiling.
Schematics of ribosome profiling strategy in WT liver (n=3), *KRAS*^{G12D} (n=2) and *MYC*^{Tg}*;KRAS*^{G12D} mice liver tumors (n=2).

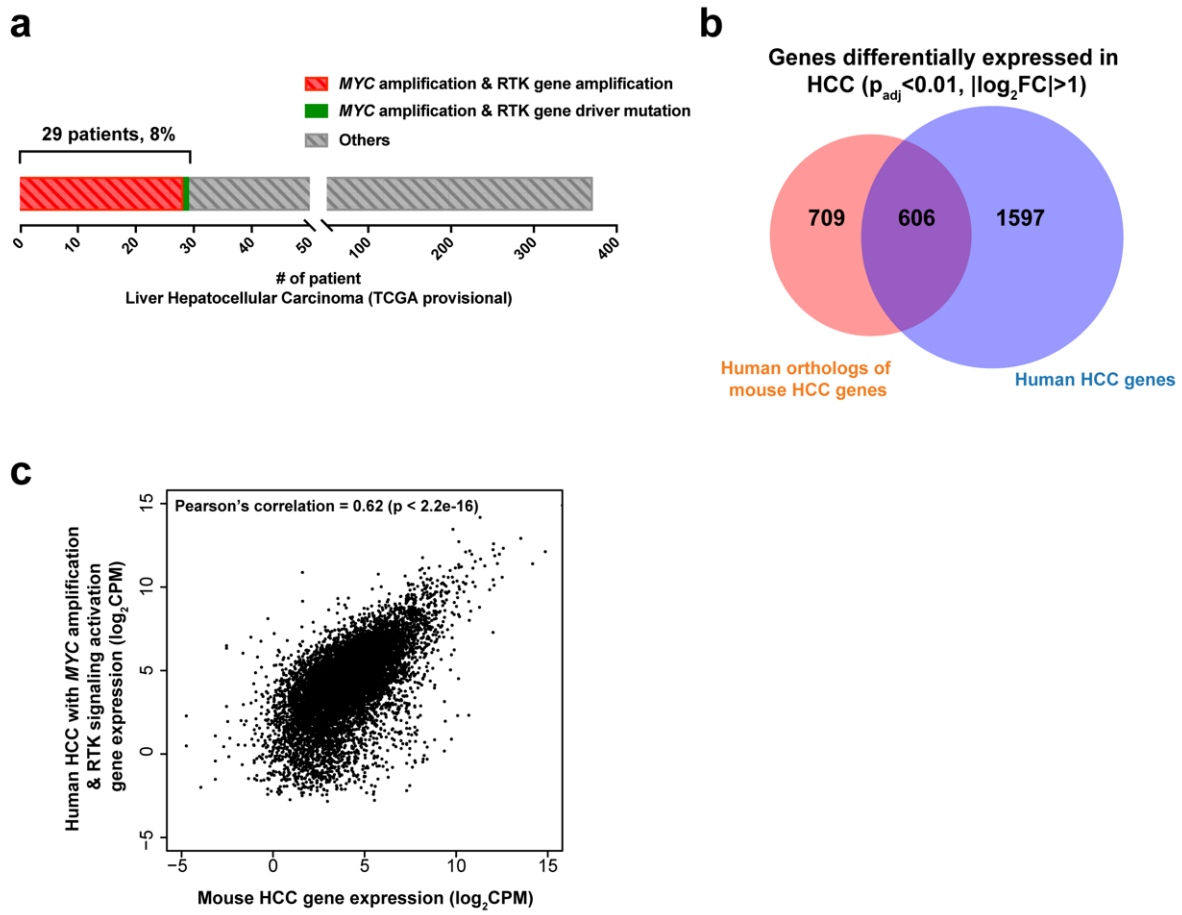

Supplementary Figure 3 The HCCs in *MYC*^{Tg};*KRAS*^{G12D} mice exhibit global transcriptional similarities to human HCCs.

(a) Graph showing 29 (out of 370) human HCC patients (8%) from the TCGA provisional liver hepatocellular carcinoma dataset harbor MYC amplification together with potential RTK signaling activation. Potential RTK signaling activation includes RTK gene copy-number amplification as well as RTK gene driver mutation with known oncogenic function.

(b) Venn diagram showing overlap of genes differentially expressed in hepatocellular carcinoma in n=29 human patients and n=2 *MYC*^{Tg}; *KRAS*^{G12D} mouse ($P = 1.07 \times 10^{-101}$, hypergeometric test), 95% confidence interval is 0.44–0.49. Differential gene expression comparing HCC to normal liver tissue samples were defined as P_{adj}<0.01 and |$\log_2$FC|>1.

(c) Comparison of gene expression levels between orthologous genes in human patients that have MYC amplification and RTK signaling activation and the *MYC*^{Tg}; *KRAS*^{G12D} mouse. The 95% confidence interval for the Pearson coefficients is 0.61–0.63 (Pearson's correlation test, two-sided $P < 2.2 \times 10^{-16}$). Average normalized gene expression levels across all tumor samples (n=29 for human and n=2 for *MYC*^{Tg}; *KRAS*^{G12D} mouse) are shown in $\log_2$CPM (counts per million).

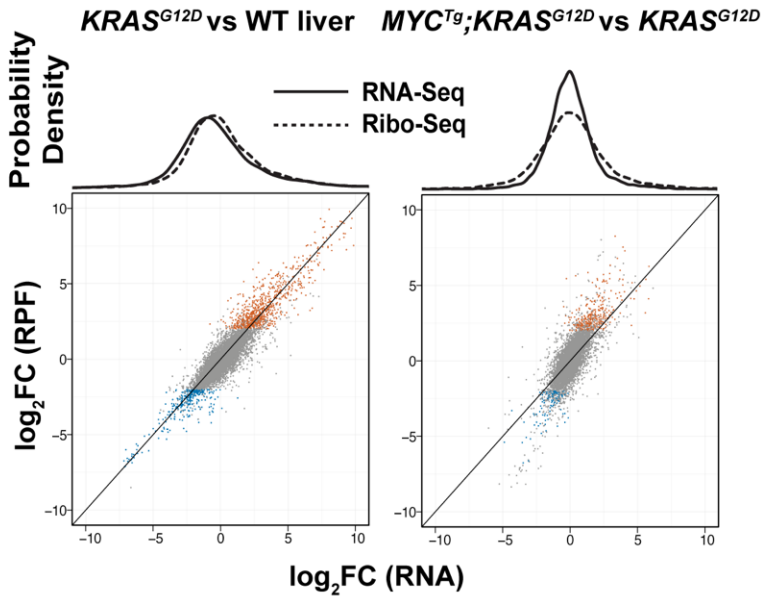

Supplementary Figure 4 Distinct from KRAS alone, MYC and KRAS cooperation selectively alters gene expression at the translation level.
Scatter plot showing the changes in Ribo-Seq (y-axis) compared to changes in RNA-Seq (x-axis), comparing *KRAS*^{G12D} (n=2) to WT (n=3) (left) and *MYC*^{Tg}*;KRAS*^{G12D} (n=2) to *KRAS*^{G12D} (n=2) (right). Genes that are significantly up or down-regulated in Ribo-Seq (P_{adj} <0.1 and |log2FC| > 2) are highlighted in orange and blue respectively. Comparison of the probability density distribution of log2FC in RNA-Seq (solid line) and Ribo-Seq (dashed line) reveals a greater alteration in the Ribo-Seq than RNA-Seq between *MYC*^{Tg}*;KRAS*^{G12D} and *KRAS*^{G12D}.

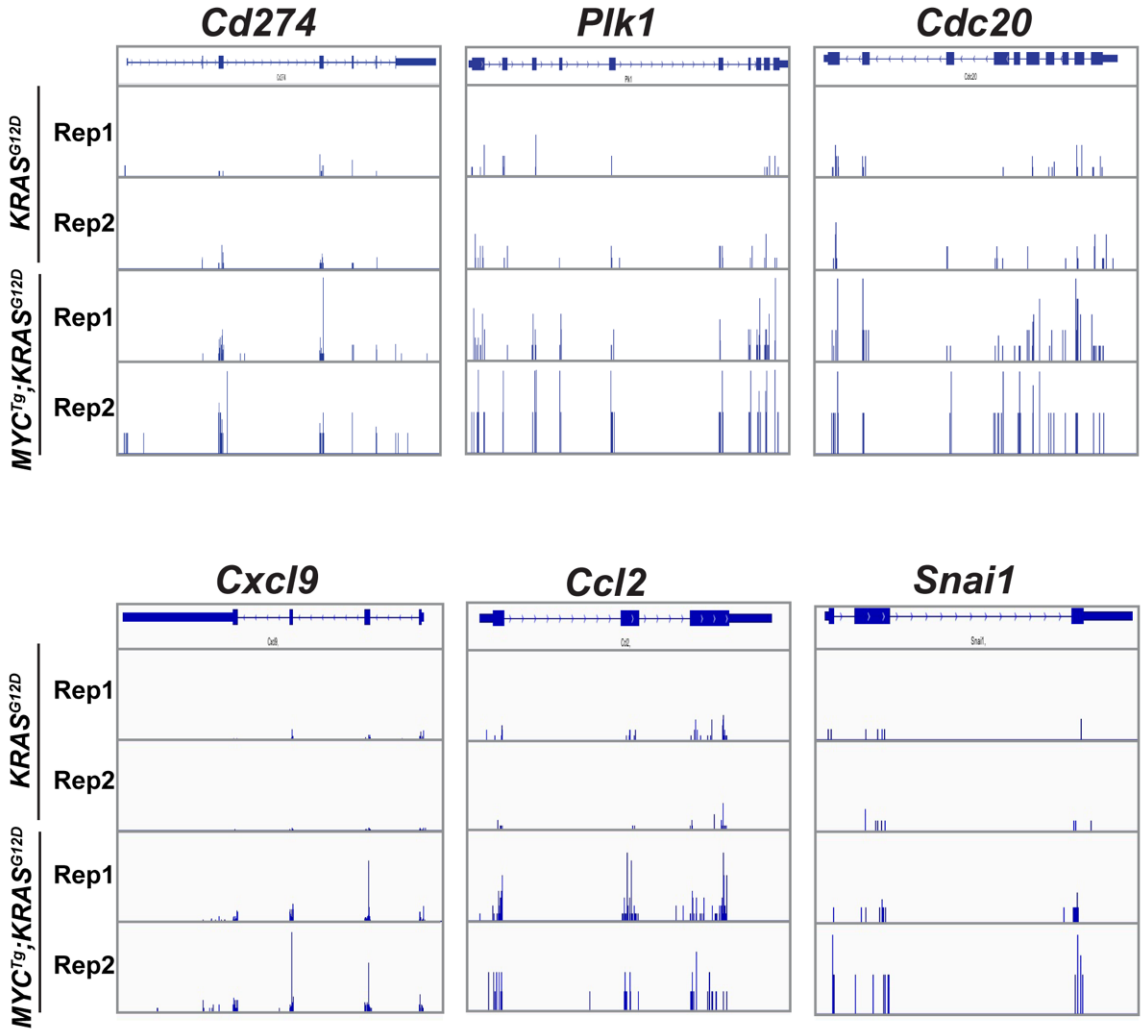

Supplementary Figure 5 Ribosome profiling indicates that *MYC* upregulates the translation of *Cd274, Plk1, Cdc20, Cxcl9, Ccl2* and *Snai1* when cooperating with *KRAS*^{G12D}.

Ribo-Seq plots of *Cd274* (gene coding PD-L1 protein), *Plk1, Cdc20, Cxcl9, Ccl2* and *Snai1* in *KRAS*^{G12D} (n=2) and *MYC*^{Tg}*; KRAS*^{G12D} (n=2) mice HCC are shown. Approximate 5-fold increase in the ribosome reads at *Cd274* mRNA is detected, in accordance to the IF result shown in Fig 2c.

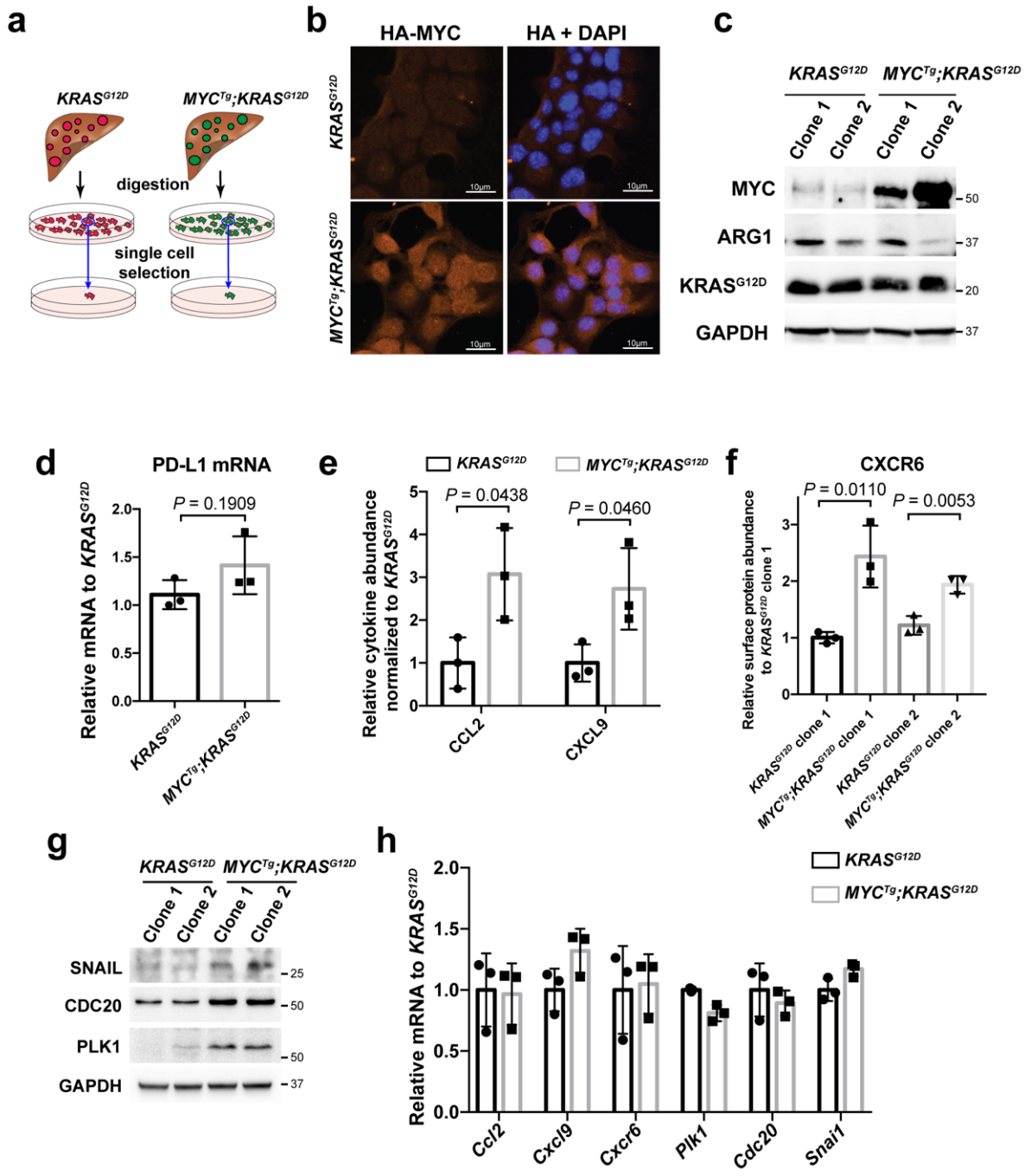

Supplementary Figure 6 MYC, in cooperation with KRAS^{G12D}, regulates genes expression at the protein levels instead of transcriptional levels in mouse HCC cells.

(a) Schematic of the protocol for generating single clone mouse liver HCC cell lines from *KRAS^{G12D}* and *MYC^{Tg};KRAS^{G12D}* liver tumors.

(b) HA-MYC and DAPI were assessed by immunofluorescence in cell lines derived from tumors of *MYC^{Tg};KRAS^{G12D}* and *KRAS^{G12D}* mice liver. Representative figure from n=3 independent experiments is shown.

(c) MYC, ARG1, KRAS^{G12D} and GAPDH proteins were assessed by western blot in single cloned cell lines derived from tumors of *MYC^{Tg};KRAS^{G12D}* and *KRAS^{G12D}* mice liver. Representative figure from n=3 independent experiments is shown.

(d) Relative mRNA expressions of PD-L1 in single cloned cell lines derived from tumors of *MYC*^{Tg}*;KRAS*^{G12D} and *KRAS*^{G12D} mice liver were assessed by RT-qPCR. n=3 independent experiments is shown, two-sided *t*-test.
(e) Relative secreted CCL2 and CXCL9 abundance in *MYC*^{Tg}*;KRAS*^{G12D} and *KRAS*^{G12D} HCC cells were assessed by flow cytometry. n=3 independent experiments is shown, two-sided *t*-test.
(f) Relative surface CXCR6 abundance in *MYC*^{Tg}*;KRAS*^{G12D} and *KRAS*^{G12D} HCC cells were assessed by flow cytometry. n=3 independent experiments is shown, two-sided *t*-test.
(g) SNAIL, CDC20, PLK1 and GAPDH protein abundance were assessed by western blot in *MYC*^{Tg}*;KRAS*^{G12D} and *KRAS*^{G12D} HCC cells. Representative figure from n=3 independent experiments is shown.
(h) Relative mRNA expressions of *Ccl2, Cxcl9, Cxcr6, Plk1, Cdc20* and *Snai1* were assessed by RT-qPCR. n=3 independent experiments is shown, two-sided *t*-test.
All values represent the mean ± SD. Uncropped blots are provided in Supplementary Figure 15.

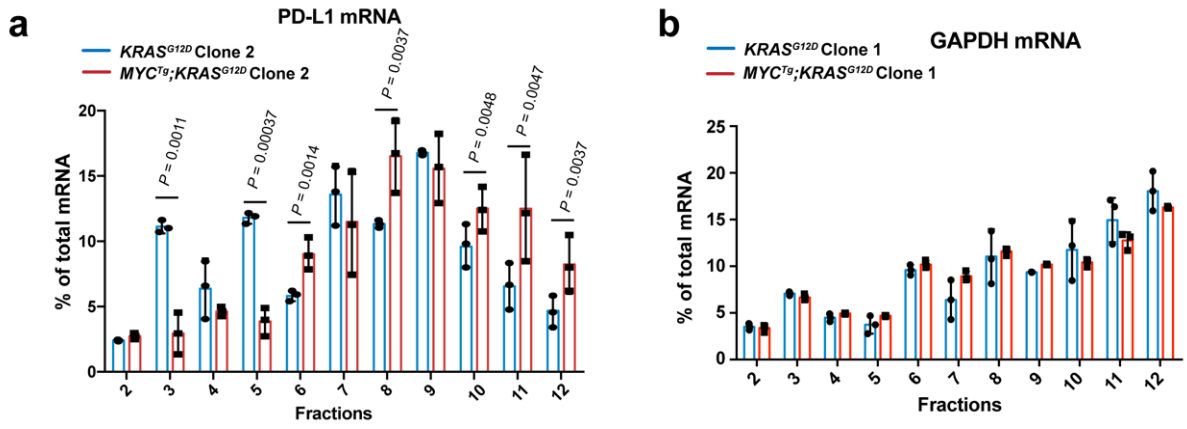

Supplementary Figure 7 MYC in cooperation with KRAS^{G12D}, upregulates PD-L1 but not GAPDH mRNA translation.

(a) RT-qPCR analysis of PD-L1 mRNA levels in fractions, percentages of PD-L1 mRNA distributed in each fraction against total PD-L1 mRNA, in *MYC*^{Tg}*;KRAS*^{G12D} and *KRAS*^{G12D} HCC cells (clone 2) are shown. n=3 independent experiments, two-sided *t*-test.

(b) RT-qPCR analysis of GAPDH mRNA levels in fractions, percentages of GAPDH mRNA distributed in each fraction against total GAPDH mRNA in *MYC*^{Tg}*;KRAS*^{G12D} and *KRAS*^{G12D} HCC cells (clone 1) are shown are shown. n=3 independent experiments, two-sided *t*-test.

All values represent the mean ± SD.

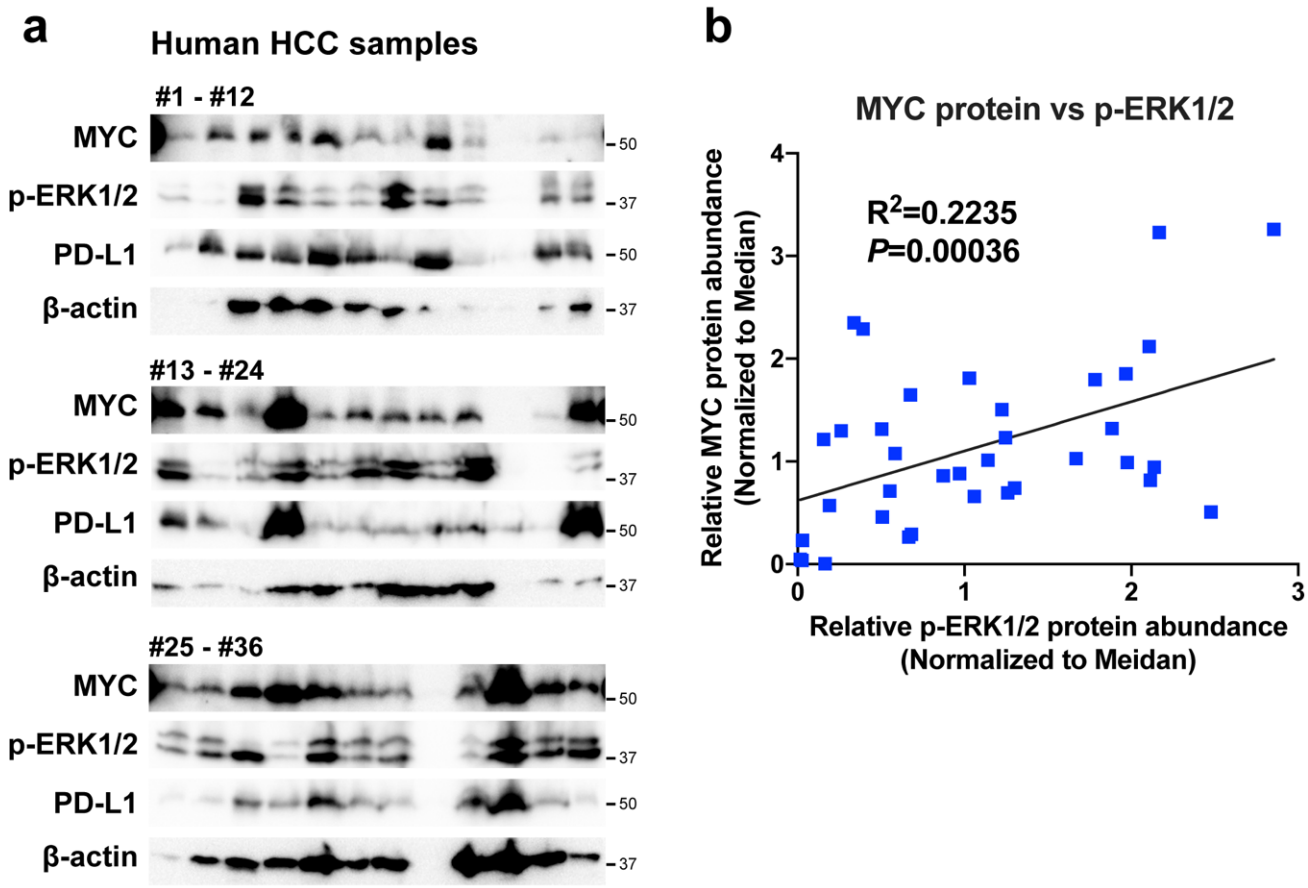

Supplementary Figure 8 MYC protein correlates with p-ERK and PD-L1 protein abundances in human HCCs.

(a) Representative western blot assessment of MYC, p-ERK1/2 and PD-L1 protein in 36 fresh frozen human HCC samples from n=3 independent experiments is shown.

(b) Comparison of relative MYC and p-ERK1/2 protein abundance (normalized to median) in n=36 fresh frozen human HCC patient samples from the western blot result in (a). The 95% confidence interval for the Pearson coefficients is 0.1707 to 0.6936 (Pearson's correlation test, two-sided P =0.0036).

Uncropped blots are provided in Supplementary Figure 15.

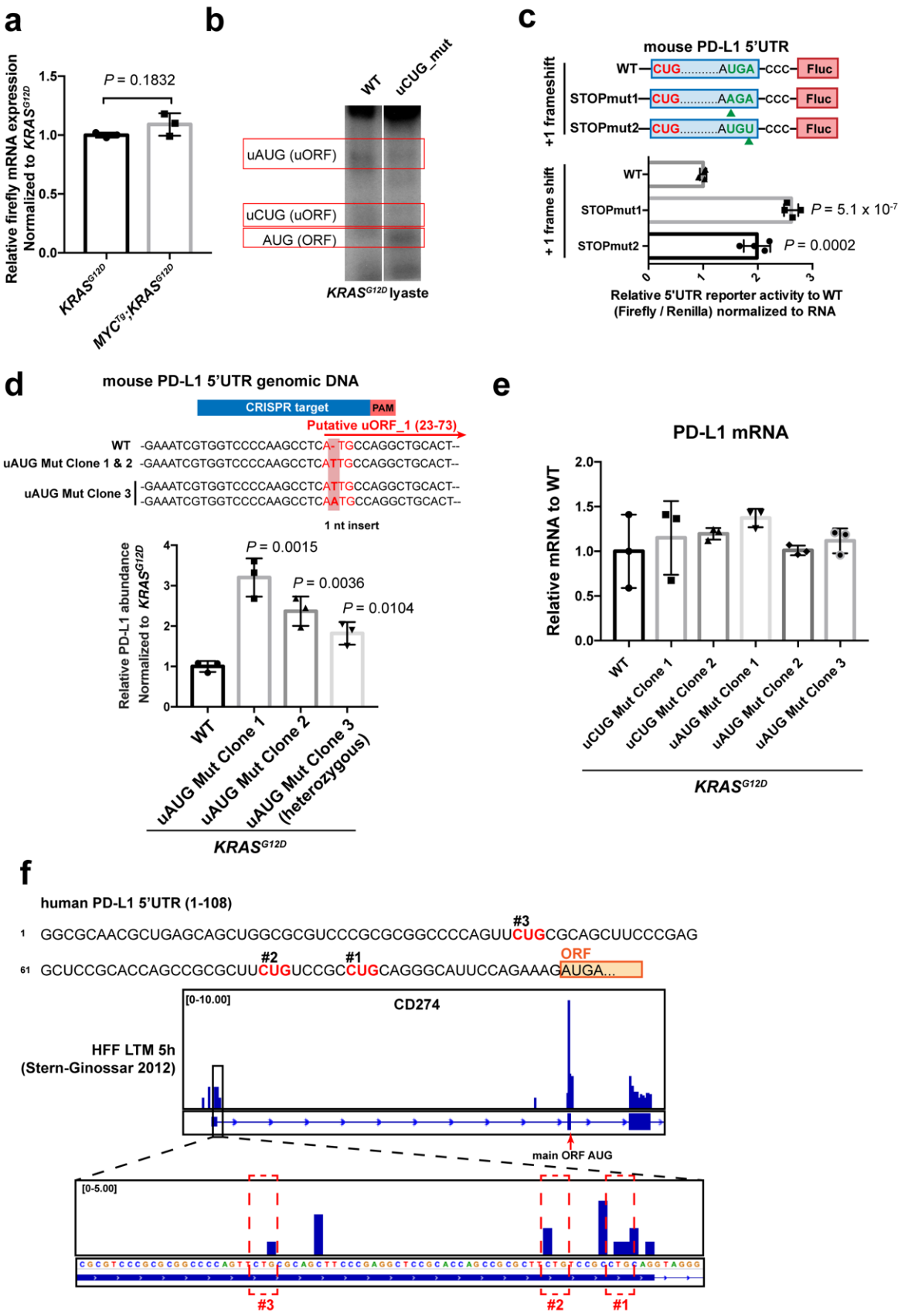

Supplementary Figure 9 uORFs within the 5' UTR of PD-L1 mRNA repress PD-L1 translation.

(a) Relative firefly mRNA levels representing the input of mRNA template for the toeprint assay using *KRAS*^{G12D} and *MYC*^{Tg}*;KRAS*^{G12D} cytoplasmic cell lysate are shown. n=3 independent experiments, two-sided *t*-test.
(b) Autoradiography of the cDNA products from the toeprint assay using cytoplasmic lysate from *KRAS*^{G12D} cells and mRNA containing WT PD-L1 5'UTR and PD-L1 5'UTRs with uCUG mutation. Representative figure from n=3 independent experiments is shown.
(c) 5' UTR reporter activity of PD-L1 uORF that is in frame with the luciferase ORF, with and without stop codon mutations (A'U'GA to A'A'GA, and AUG'A' to AUG'U'), in *KRAS*^{G12D} cells. n=4 independent experiments, two-sided *t*-test.
(d) Up: Mouse PD-L1 5'UTR exon DNA sequence of the WT and uAUG mutation *KRAS*^{G12D} clonal cell line are shown. PAM region is highlighted in red, CRISPR target region in blue. 1nt insertion is detected within the uAUG start codon (Clone 1 and 2 are homozygous; Clone 3 is heterozygous). Down: Relative PD-L1 abundance in WT and three mutation clonal cell lines determined by flow cytometry. n=3 independent experiments, two-sided *t*-test.
(e) Relative PD-L1 mRNA expressions in WT and two *KRAS*^{G12D} cell lines with uCUG or uAUG mutations were assessed by RT-qPCR. n=3 independent experiments, two-sided *t*-test.
(f) Upper panel: The sequence of human PD-L1 5'UTR. Putative uORFs start codons- uCUGs are highlighted in red. Lower panel: Ribo-Seq plots of *CD274* in human foreskin fibroblast (HFF) treated with Lactimidomycin (LTM). Initiation ribosome footprints are detected around the uCUGs.
Data represent the mean ± SD. Uncropped blots are provided in Supplementary Figure 15.

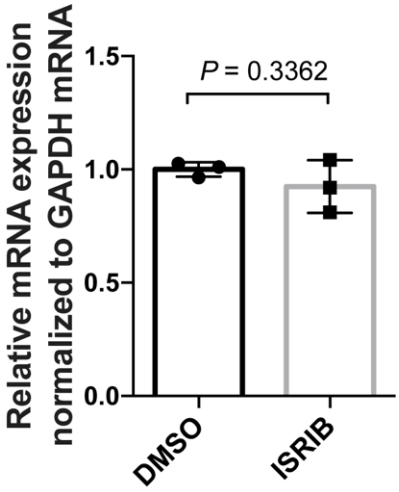

Supplementary Figure 10 PD-L1 mRNA expression is not regulated by ISRIB.
Relative PD-L1 mRNA expression in $MYC^{Tg};KRAS^{G12D}$ cell lines treated with DMSO or ISRIB for 48 hours. n=3 independent experiments, two-sided *t*-test. Data represent the mean ± SD.

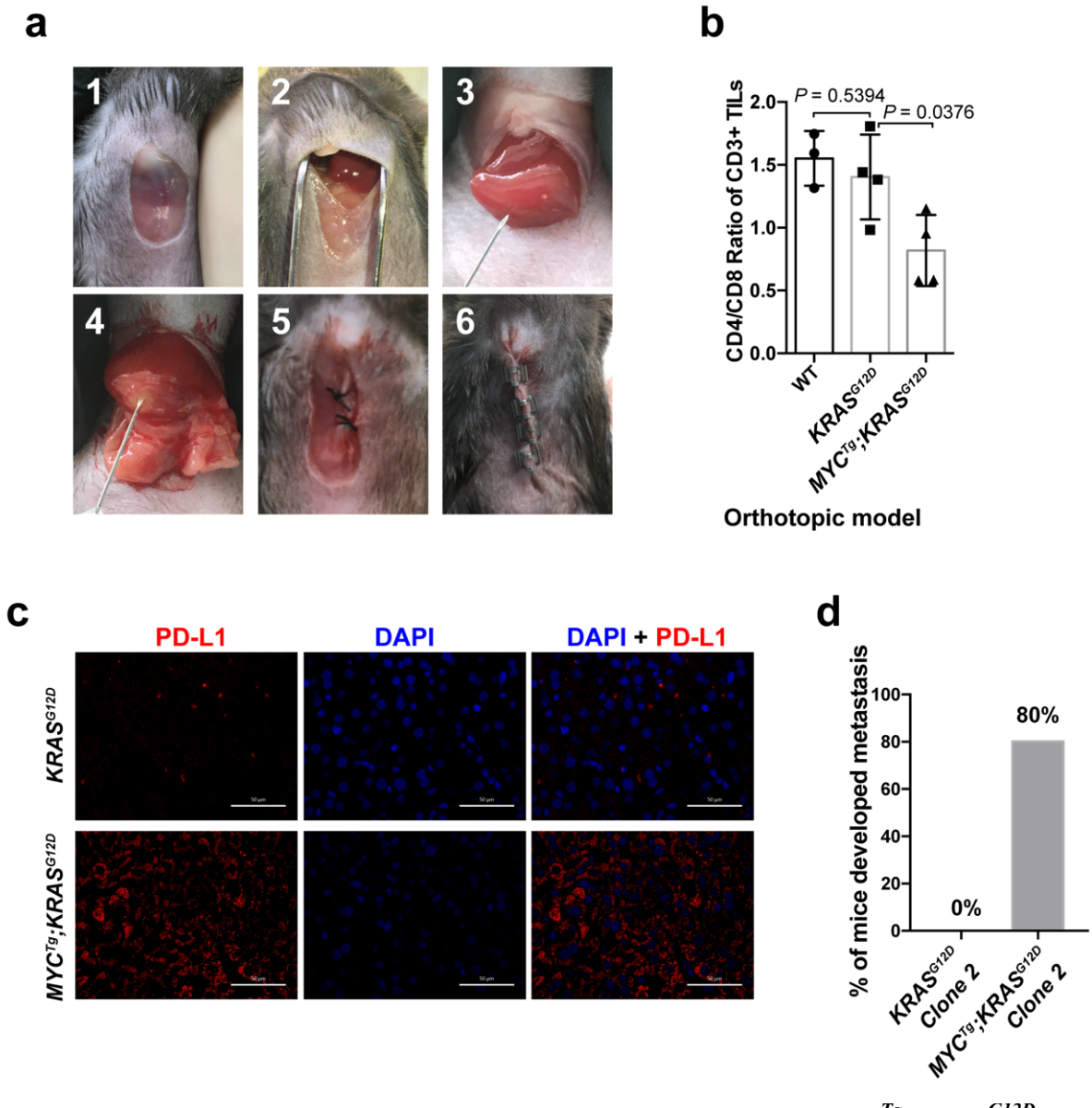

Supplementary Figure 11 Generation and characterization of *MYC^{Tg};KRAS^{G12D}* and *KRAS^{G12D}* orthotopic mice liver cancer models.

(a) Graphs showing the procedures of orthotopical injection of *MYC^{Tg};KRAS^{G12D}* and *KRAS^{G12D}* cells into the livers of C57/B6 mice.

(b) CD4/CD8 T-cell ratio in the livers of WT (n=3) mice and mice injected with *MYC^{Tg};KRAS^{G12D}* (n=4) and *KRAS^{G12D}* cells (n=4). Two-sided *t*-test.

(c) Representative PD-L1 and DAPI immunofluorescence staining of the livers of mice injected with *MYC^{Tg};KRAS^{G12D}* and *KRAS^{G12D}* cells from n=3 independent experiments is shown.

(d) Percentage of C57BL/6 mice injected with *KRAS^{G12D}* clone 2 (n=5) and *MYC^{Tg};KRAS^{G12D}* clone 2 (n=5) cells developed metastasis.

Data represent the mean ± SD.

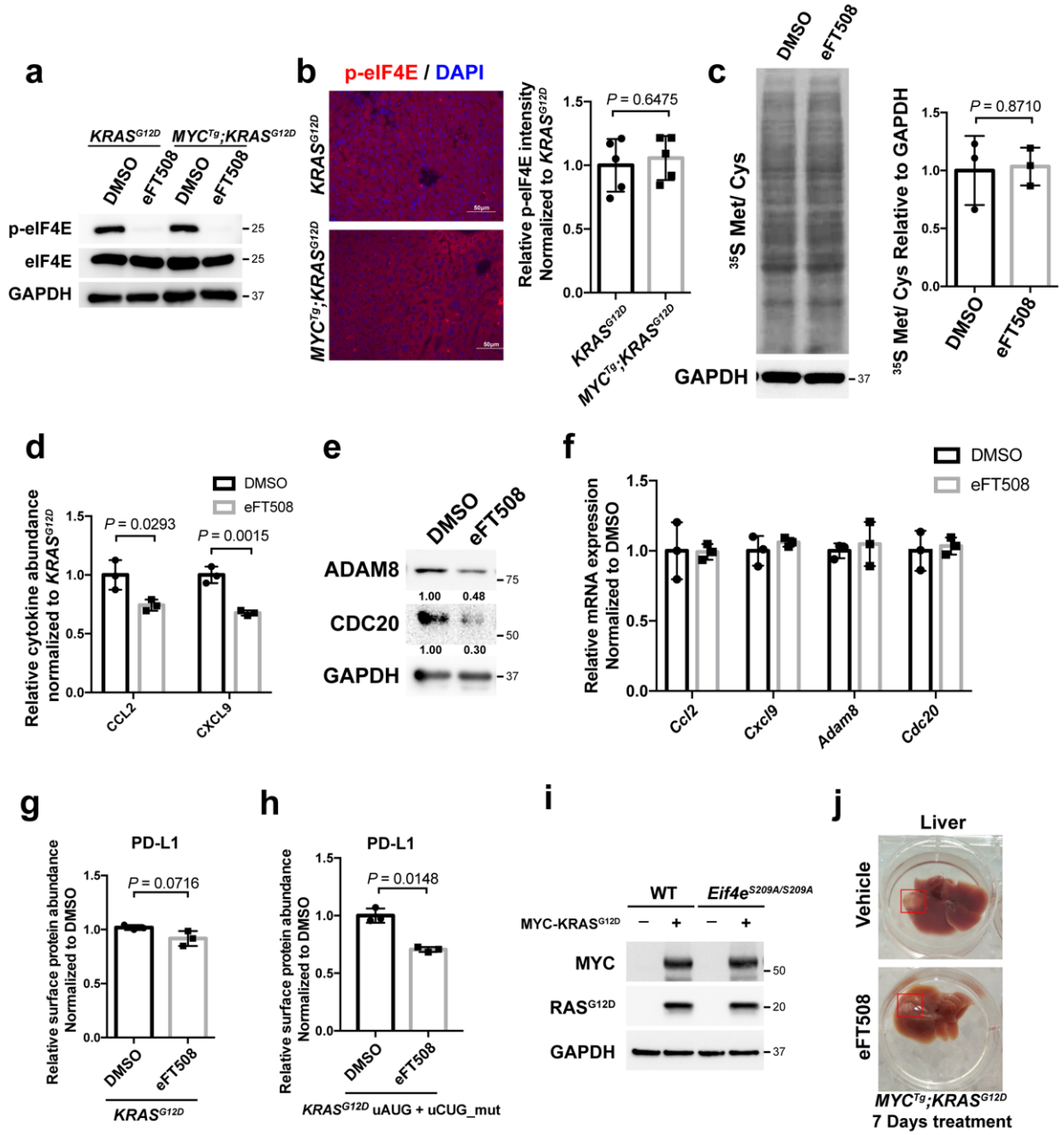

Supplementary Figure 12 MNK1/2 inhibitor eFT508 selectively reduces PD-L1 and other protein abundance in *MYC^{Tg};KRAS^{G12D}*, resulting in tumor regression.

(a) Western blot of p-eIF4E, eIF4E and GAPDH in *KRAS^{G12D}* and *MYC^{Tg};KRAS^{G12D}* cell lines. Representative figure from n=3 independent experiments is shown.

(b) Left: representative p-eIF4E and DAPI immunofluorescence staining of the livers of mice injected with *MYC^{Tg};KRAS^{G12D}* and *KRAS^{G12D}* cells. Right: quantification of relative p-eIF4E intensity relative to the *KRAS^{G12D}*. n=5 animals, two-sided *t*-test.

(c) Protein synthesis was measured by [^{35}S]-methionine incorporation of newly synthesized proteins in *MYC^{Tg};KRAS^{G12D}* cells treated with inhibitors of eFT508. Quantifications are shown on the right. n=3 independent experiments, two-sided *t*-test.

(d) Relative secreted CCL2 and CXCL9 abundance in *MYC^{Tg};KRAS^{G12D}* cells upon 72h DMSO or eFT508 treatment were assessed by flow cytometry. n=3 independent experiments, two-sided *t*-test.

(e) ADAM8, CDC20, and GAPDH protein abundances were assessed by western blot in *MYC*^{Tg};*KRAS*^{G12D} and *KRAS*^{G12D} HCC cells upon 72h DMSO or eFT508 treatment. Representative figure from n=3 independent experiments is shown.
(f) Relative mRNA expressions of *Ccl2, Cxcl9, Adam8*, and *Cdc20* were assessed by RT-qPCR. n=3 independent experiments, two-sided *t*-test.
(g) Relative surface PD-L1 abundance assessed by flow cytometry in *KRAS*^{G12D} cell lines treated with DMSO or eFT508 for 72 hours. n=3 independent experiments, two-sided *t*-test.
(h) Relative surface PD-L1 abundance assessed by flow cytometry in *KRAS*^{G12D} cells with both uAUG and uCUG mutations (*KRAS*^{G12D} uAUG+ uCUG_mut) treated with DMSO or eFT508 for 72 hours. n=3 independent experiments, two-sided *t*-test.
(i) Western blot of MYC, RAS^{G12D} and GAPDH in vector or *MYC* and *KRAS*^{G12D} overexpressed hepatocytes of WT and *Eif4e*$^{S209A/S209A}$ mice. Representative figure from n=3 independent experiments is shown.
(j) Representative figures of mouse livers injected with *MYC*^{Tg};*KRAS*^{G12D} cells for 7 days followed by 7-day Vehicle (n=10 animals) or eFT508 (n=6 animals) treatment. Red box highlights the tumors formed.
Data represent the mean ± SD. Uncropped blots are provided in Supplementary Figure 15.

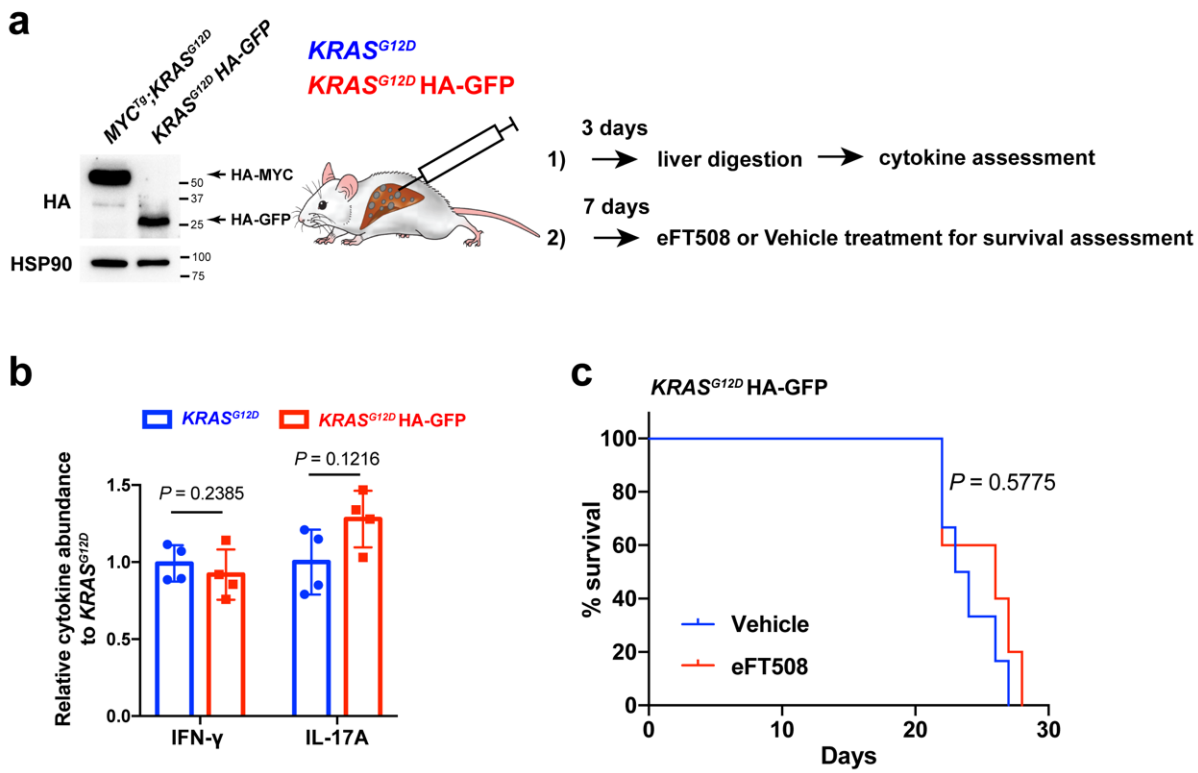

Supplementary Figure 13 HA-tag does not induce antigen-specific Th1 response or affect the tumor sensitivity to eFT508.

(a) Left: Representative western blot of HA and HSP90 (control) in $MYC^{Tg};KRAS^{G12D}$ and $KRAS^{G12D}$ cells stably overexpressing HA-tagged GFP from 3 independent experiments. The HA level overexpressed in $KRAS^{G12D}$ cells is comparable to that in $MYC^{Tg};KRAS^{G12D}$ cells. Right: $KRAS^{G12D}$ and $KRAS^{G12D}$ cells stably overexpressing HA-tagged GFP were injected into the liver of C57/BL6 mice with indicated follow-up assays and treatments.

(b) IFN-γ and IL-17A abundance in the liver of mice injected with $KRAS^{G12D}$ cells and $KRAS^{G12D}$ cells stably overexpressing HA-tagged GFP were assessed by flow cytometry. n=4 animals, two-sided *t*-test. Data represent the mean ± SD.

(c) Kaplan–Meier curves showing the survival of male C57/B6 mice with $KRAS^{G12D}$ HA-GFP cells orthotopically injected into the livers. Vehicle (n=6 animals) or eFT508 (10 mg/kg) (n=5 animals) was orally administered once a day starting 7-day post-tumor implantation. Wilcoxon rank sum test.

Uncropped blots are provided in Supplementary Figure 15.

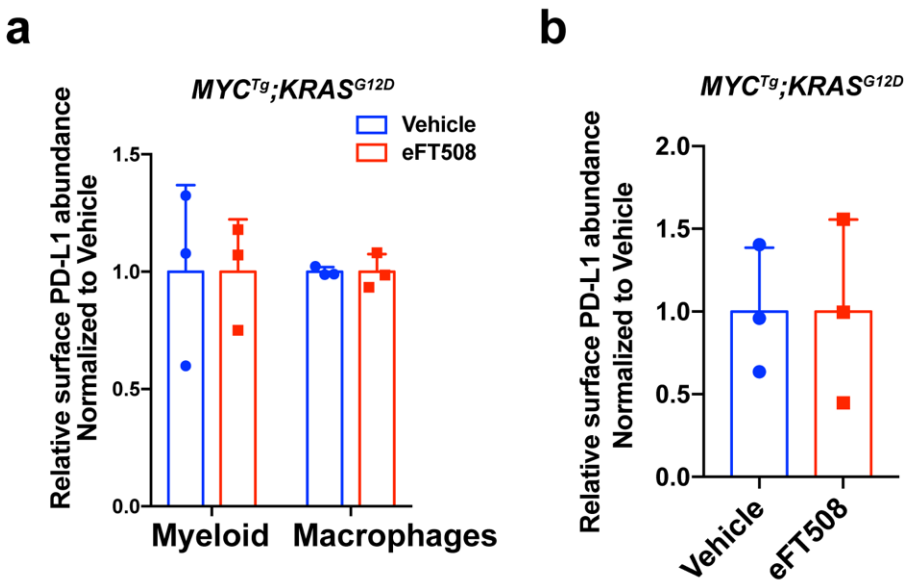

Supplementary Figure 14 eFT508 has limited effect on reducing PD-L1 protein abundance in tumor-infiltrated immune cells.

Male C57/B6 mice with *MYC*^{Tg};*KRAS*^{G12D} cells orthotopically injected into the livers. Vehicle (n=3 animals) or eFT508 (10 mg/kg) (n=3 animals) was orally administered once a day starting 7 days post-tumor implantation. (a) Relative surface PD-L1 abundance assessed by flow cytometry on tumor infiltrated myeloid cells and liver-resident macrophages with vehicle or eFT508 treatment. Two-sided *t*-test.

(b) Relative surface PD-L1 abundance on isolated T lymphocytes from the mice livers injected with *MYC*^{Tg};*KRAS*^{G12D} cells followed by 7-day vehicle (n=3 animals) or eFT508 (n=3 animals) treatment were assessed by flow cytometry. Two-sided *t*-test.

Data represent the mean ± SD.

Supplementary Figure 15 Uncropped immunoblot pictures.

Figure 3b

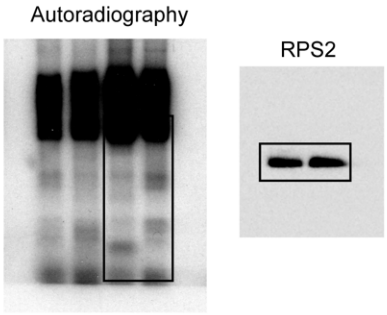

Figure 3f

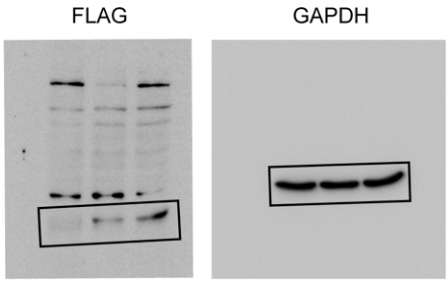

Figure 3i

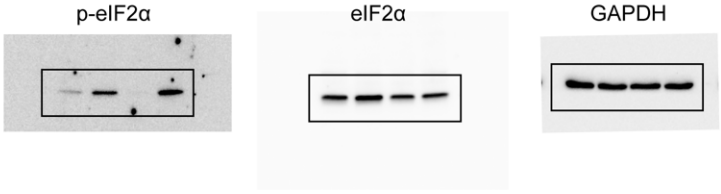

Supplementary Figure 1b

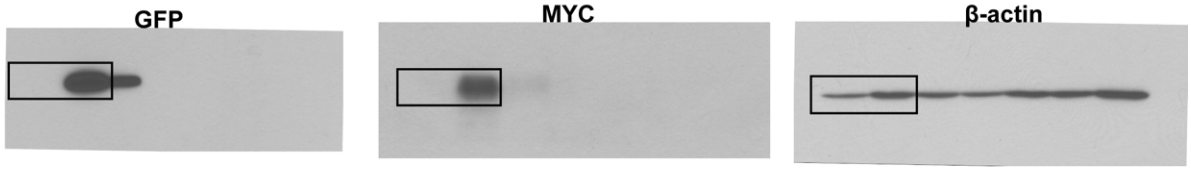

Supplementary Figure 5c

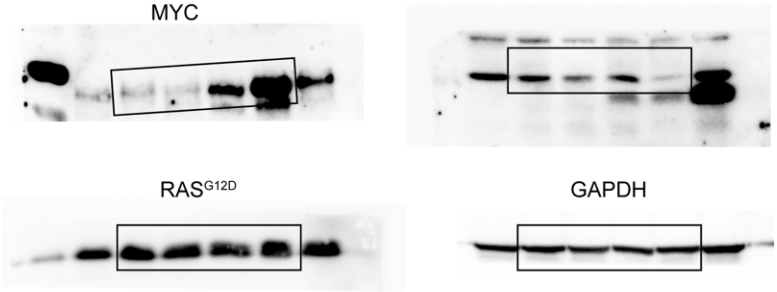

Supplementary Figure 5g

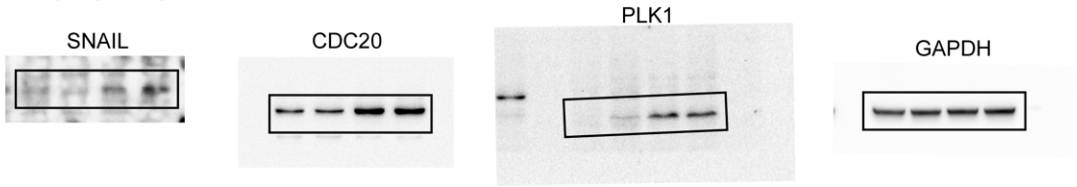

Supplementary Figure 15 Uncropped immunoblot pictures.

Supplementary Figure 7a

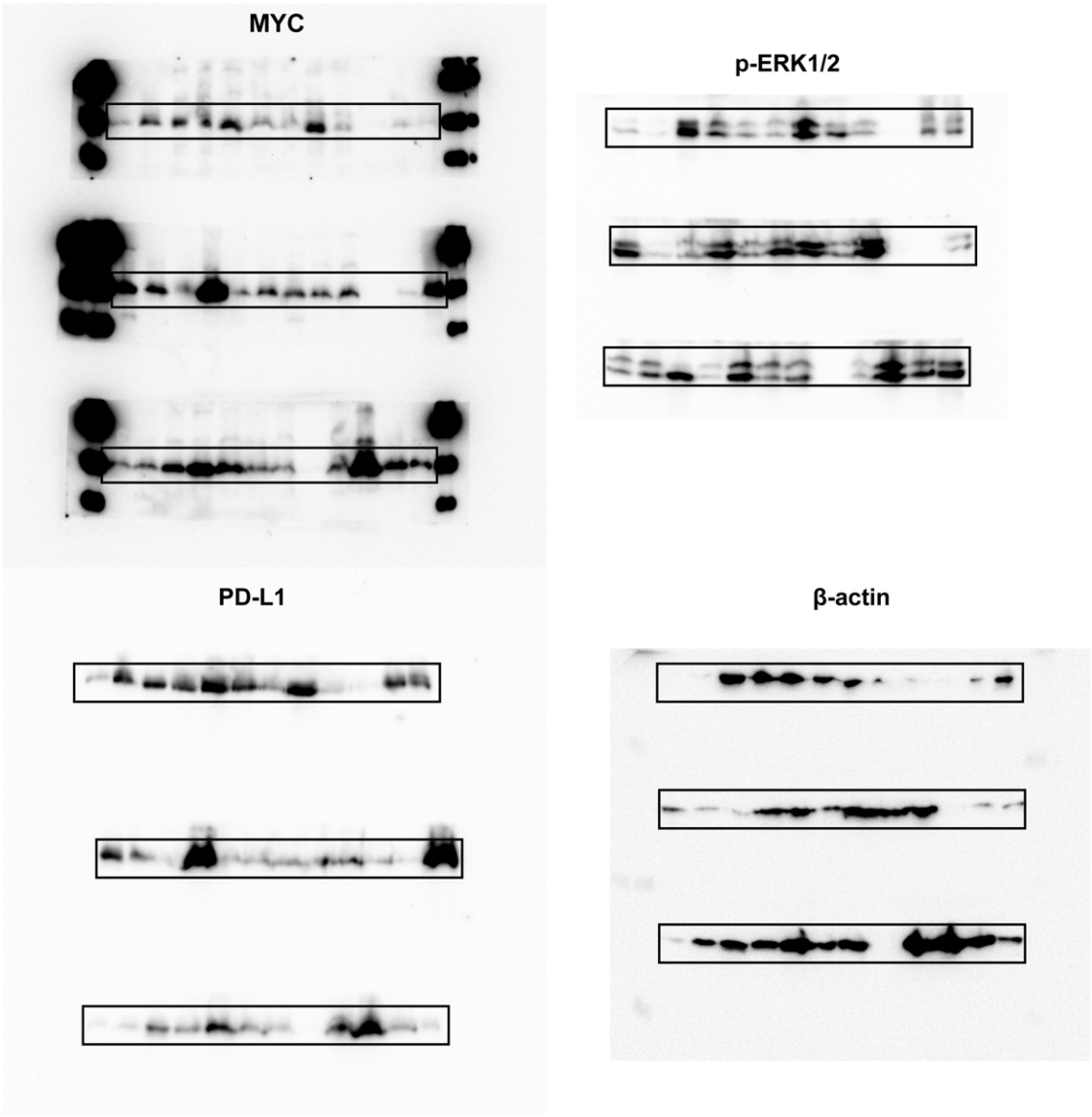

Supplementary Figure 8b

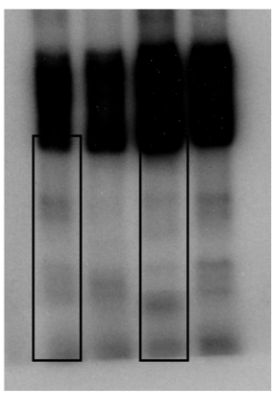

Supplementary Figure 15 Uncropped immunoblot pictures.

Supplementary Figure 11a

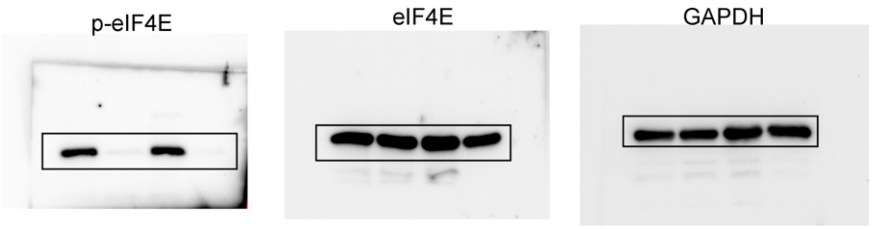

Supplementary Figure 11c

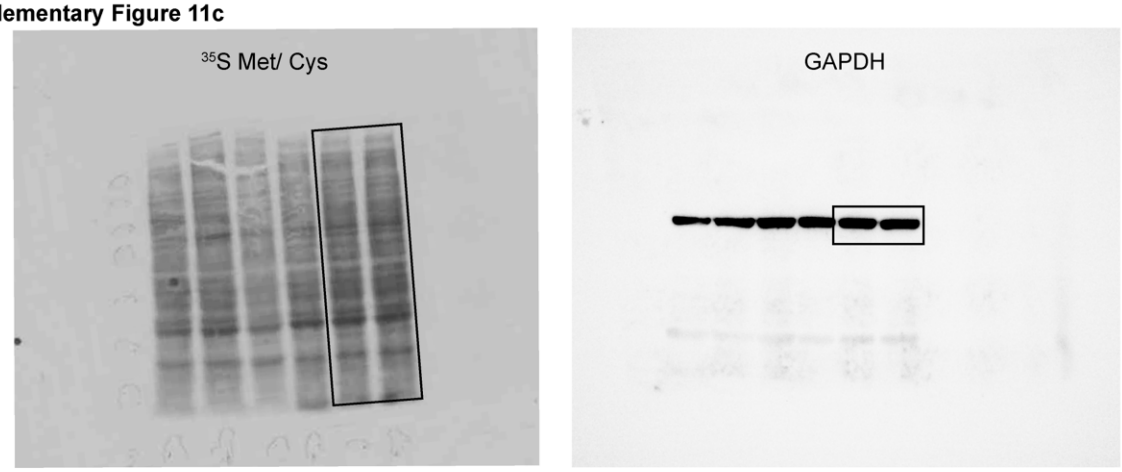

Supplementary Figure 11e

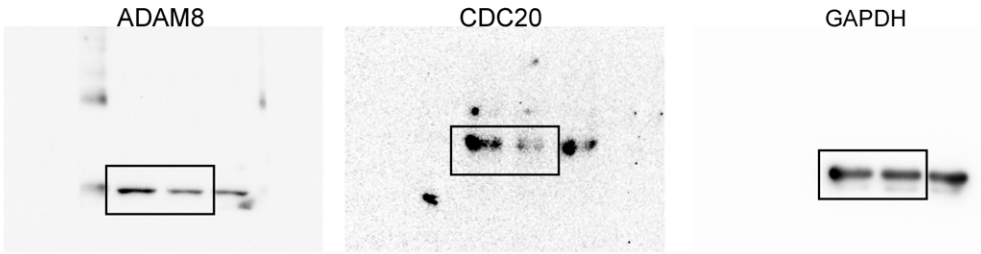

Supplementary Figure 11i

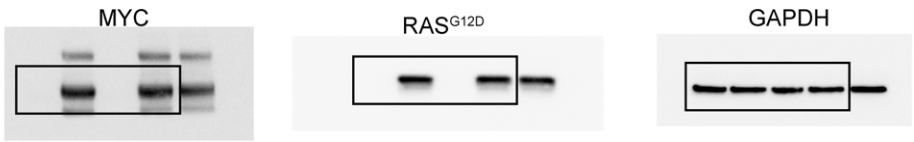

Supplementary Figure 12a